Potent Non-Nucleoside Inhibitors of the Measles Virus RNA-Dependent RNA Polymerase Complex

Aiming Sun,*,† Jeong-Joong Yoon,‡ Yan Yin,† Andrew Prussia,† Yutao Yang,† Jaeki Min,† Richard K. Plemper,‡ and James P. Snyder*,†

Department of Chemistry, Emory University, 1515 Dickey Drive, Atlanta, Georgia 30322, Department of Pediatrics, Division of Pediatric Infectious Diseases, Emory Children's Center, Emory University School of Medicine, 2015 Uppergate Drive, Atlanta, Georgia 30322

Received October 5, 2007

Measles virus (MV) is one of the most infectious pathogens known. In spite of the existence of a vaccine, approximately 350000 deaths/year result from MV or associated complications. Antimeasles compounds could conceivably diminish these statistics and provide a therapy that complements vaccine treatment. We recently described a high-throughput screening hit compound **1** (16677) against MV-infected cells with the capacity to eliminate viral reproduction at 250 nM by inhibiting the action of the virus's RNA-dependent RNA polymerase complex (RdRp). The compound, 1-methyl-3-(trifluoromethyl)-*N*-[4-sulfonylphenyl]-1*H*-pyrazole-5-carboxamide, **1** carries a critical CF_3 moiety on the 1,2-pyrazole ring. Elaborating on the preliminary structure−activity (SAR) study, the present work presents the synthesis and SAR of a much broader range of low nanomolar nonpeptidic MV inhibitors and speculates on the role of the CF_3 functionality.

Introduction

Paramyxoviruses are negative stranded RNA viruses, most of which are highly contagious airborne pathogens that spread via the respiratory route. Members of this viral family include major human and animal pathogens such as measles virus (MV),[a] human parainfluenza viruses (HPIV), mumps virus, respiratory syncytial virus, and Newcastle disease virus.[1] Despite the existence of an effective live-attenuated vaccine,[2] MV remains a serious threat to human health globally, accounting for approximately 0.35 million deaths annually.[3] While most of these cases occur in developing countries with limited access to vaccination, measles outbreaks still occur in some developed countries that have failed to maintain high vaccine coverage rates. According to recent estimates, 20 million cases of measles occur annually worldwide. Current outbreaks in the developed world have affected Japan in the Western Pacific Region, Nova Scotia, New Brunswick, Prince Edward Island, and Ontario, Canada, and several parts of Western Europe.[4,5a–c]

This is partially due to declining herd immunity as a result of reduced vaccination coverage resulting from parental concerns about vaccination safety.[6] Vaccination coverage below protective levels in areas of the developing world and continued viral activity in the developed world make desirable the development of novel therapeutics that can be used for the rapid control of local outbreaks and improved case management to limit severe outcomes of infection.

To date, ribavirin is the only drug available for the treatment of some paramyxovirus infections[7,8] It has been used experimentally for the treatment of measles but with limited efficacy.[9] More recently, benzimidazothiazole derivatives have been reported to be more potent and less cytotoxic compared with ribavirin against the Leningrad 16 strain, when assessed in Vero (African green monkey kidney carcinoma) cells. The most active compound in this series demonstrated a selectivity ratio (CC_{50}/EC_{50}) of 245.5 compared with 14.4 for ribavirin.[10]

In previous work, we reported the structure-based development of a MV entry inhibitor, compound **30** (AS-4,[11,12] Figure 1), with an EC_{50} of 260 nM against the MV-Edmonston (MV-Edm) strain. Because this compound proved to be unstable, we developed nitro analogue **31** (AS-48) with an EC_{50} of 0.6−3.0 μM (Figure 1) as a shelf-stable alternative.[11b] Further attempts to increase the activity within this series of compounds proved to be problematic. As a consequence, we broadened our search by turning to cell-based high-throughput screening (HTS) to capture small molecules capable of netting both entry inhibitors as well as compounds operating against other proteins critical for viral infection and reproduction. The exercise identified 1-methyl-3-(trifluoromethyl)-*N*-[4-(pyrrolidinylsulfonyl)phenyl]-1*H*-pyrazole-5-carboxamide **1** (16677) (Figure 1) (EC_{50} = 250 nM,) as a well-behaved, target-specific inhibitor of MV replication.[13] Bypassing the fusion protein, **1** represents a first-in-class non-nucleoside inhibitor of the MV RNA-dependent RNA polymerase (RdRp) complex. Following resynthesis of the hit compound **1**, by coupling 1-methyl-3-trifluoro-pyrazole-5-acetyl chloride with 4-amino-prolidinyl sulfonamide **7a** in the presence of pyridine,[14,31] previous preliminary structural modifications focused on the right side of the molecule as depicted in Figure 2(b).[15] In the present work, we describe optimization of antiviral activity for compound **1** scaffold by manipulation of the pyrazole (A) and pyrrolidine (D) rings.

Preparation of Analogues around the HTS Hit Compound 1. Modification of the Pyrazole Ring. The first stage of hit optimization introduced a variety of aromatic rings as 1-methyl-3-trifluoromethyl pyrazole replacements. Compounds **2a**−**o** (Figure 2b, Table S1, Supporting Information) can be readily prepared by coupling the corresponding acid chlorides with 4-amino-prolidinyl sulfonamide **7a** in the presence of pyridine.[15] Preliminary efforts were also devoted

* To whom correspondence should be addressed. Phone: 404-727-6689 (A.S.); 404-727-2415 (J.P.S.). Fax: 404-727-6689 (A.S.); 404-727-6586 (J.P.S.). E-mail: asun2@emory.edu (A.S.); jsnyder@emory.edu (J.P.S.).

† Department of Chemistry, Emory University.

‡ Department of Pediatrics, Division of Pediatric Infectious Diseases, Emory Children's Center, Emory University School of Medicine.

[a] Abbreviations: MV, measles virus; CPE, cytopathic effect; MTT, [3-(4,5-dimethylthiazol-2-yl)-2,5-diphenyltetrazolium bromide]; MV-Edm, measles virus Edmonston strain; RdRp, RNA-dependent RNA polymerase; CC_{50}, compound concentration that returns 50% cytotoxicity; EC_{50}, compound concentration that returns 50% inhibition; SI, selectivity index, defined as CC_{50}/EC_{50}; SAR, structural activity relationship; QSAR, quantitative structural activity relationship; MFTA, molecular field topology analysis.

10.1021/jm701239a CCC: $40.75
Published on Web 06/05/2008

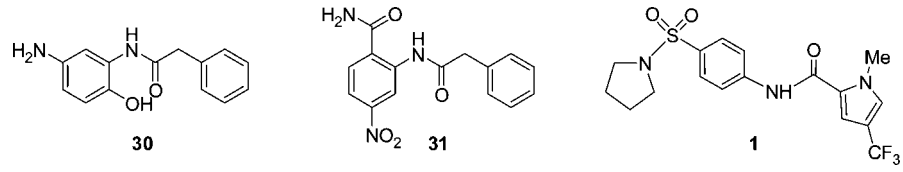

Figure 1. Structures of previous measles virus entry inhibitors (**30**, **31**) and hit compound **1**.

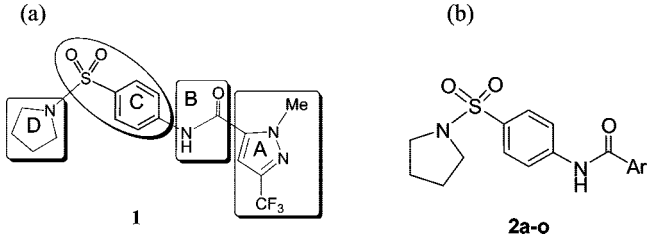

Figure 2. (a) Sectors of compound **1** utilized as an SAR template. (b) Aromatic ring analogues of the compound **1** pyrazole ring, **2a**−**o**.

to modifying the 1-methyl-3-trifluoromethyl-pyrazole ring. For example, the corresponding 4-bromo-1-methyl-3-(trifluoromethyl)-*1H*-pyrazole-5-carboxylic acid was prepared by the protocol reported by Schlosser and treated with oxalyl chloride to obtain acid chloride **3**.[14] The latter was further coupled with sulfonamide **7a** to give the 4-bromo-substituted analogue **4** (Scheme 1).

In the present work, 3-trifluoromethyl pyrazole was treated with NaH in DMF, followed by regioselective benzylation and alkylation to obtain 1-benzyl or alkyl-3-trifluoromethylpyrazole. The compound was then subjected to a routine deprotonation−carboxylation sequence before coupling with aniline **7c** to obtain the desired compound **9** (Scheme 2).

2-Methoxycarbonylphenyl and 2-carboxyphenyl analogues were also prepared as outlined in Scheme 3. The furan precursor **10** was obtained as previously described[16] and converted to ester **11** via the acid chloride/methylation method. Oxidation of the furyl functionality afforded the desired carboxylic acid **12**. The latter as its acid chloride was coupled to aniline **7a** to afford compound **13**. Saponification of ester **13** provided the corresponding acid **14**.

Syntheses of **23**, **24**, **28**, and **29** proved to be straightforward by following standard procedures for sulfonamide analogues as illustrated in Schemes 4 and 5. For example, combination of 4-nitro-benzenesulfonyl chloride with pyrrolidine afforded 4-nitro-pyrrolidinyl sulfonamide **6**. The latter was reduced either with $SnCl_2$ in EtOAc or by hydrogenation over Pd/C (5%) to obtain 4-amino-prolidinyl sulfonamide **7** in almost quantitative yield. Other secondary amides behave similarly. Coupling of **7** with 1-methyl-3-(trifluoromethyl)-1*H*-pyrazole-5-carbonyl chloride obtained compound **23**. Deprotection of Boc-groups with a mixture of TFA and CH_2Cl_2 (3:1) at room temperature for about 4 h delivers free amines **24e** and **24f**. Compounds **29e** and **29f** were obtained by hydrolysis of the corresponding esters **28** in 1 N HCl. Analogues **15a**−**r**[15] (See Table 1) were prepared by using the same procedure as described in Scheme 4.

Qualitative SAR for Compound 1 Analogues. Disappointedly, all attempts to replace the pyrazole ring with five- or six-membered aromatic rings[15] or to alter substitutents on the pyrazole ring (e.g., **4**, **13**, and **14**) led either to a decrease or to a complete loss of activity. A striking example is the inactivity of the series of *N*-alkyl analogues of **1** (EC_{50} 30−150 nM[15]). Replacement of the *N*-methyl with *N*-isopropyl or *N*-benzyl (**9b** and **c**, respectively) leads to disppearance of potency in the virus titer reduction assay. While the *N*-ethyl pyrazole **9a** demonstrates good activity in (EC_{50} = 55 nM), the compound is highly toxic. In a previous limited exploration of the SAR of **1**, we learned that installing a piperidine ring instead of the pyrrolidine ring on the left side of the molecule (Figure 2a, D ring) provided a 100-fold boost in activity while simultaneously delivering very low toxicity.[15] To exploit this potency advantage, a variety of alicyclic heterocyclic rings (**15a**−**l**) or dialkyl amines (**15m**−**r**) were employed as pyrrolidine replacements while retaining the remainder of compound **1** structure (see Table 1).

Piperidine analogues **15a**−**e** and **15k** exhibit significant potency improvements by comparison with the original hit. All yield EC_{50}s in the low nM range. The 2-ethyl substitution on the piperidine ring in **15e** elicits 2−6-fold less activity than methyl substitution (**15b**−**15d**). The seven-membered ring variant **15f** is 10-fold more potent than the azacyclooctane analogue **15g** and about 3-fold more active than the piperidine **15a**. However, C2-substitution of the pyrrolidine ring with either an ester or a carboxylic acid (**15h** and **15i**, respectively) greatly decreases activity by about 100-fold as does introduction of an indole ring (**15j**). Interestingly, while the open-chain diethyl amine compound **15n** is highly active, the alkyl-enhanced diisopropyl, dipropyl, and diallyl variants **15o**, **15p**, and **15r** lose 10−20 fold potency by comparison. Similarly, **15m** and **15q**, the dimethyl and di-isobutyl analogues, respectively, exhibit drops in activity.

Additional structural modifications of compound **1** included synthesis of **16**−**20**, compounds that examine structural environments around a six-membered ring. (Figure 3) Analogue **16** moves the nitrogen out of the piperidine ring of **15a** and introduces a secondary amine as an H-bond donor, while **17** incorporates a sulfonate moiety instead of a sulfonamide group. Compound **18** incorporates a methyl group on the amide and eliminates possible hydrogen bonding of NH with a nearby amino acid residue. All three compounds **16**, **17**, and **18** occasion a complete loss of activity. Compounds **19** and **20** switch the sulfonamide *para*-amide linker in sector C to the *meta*- and *ortho*-positions, respectively. Both compounds **19** and **20** similarly show no detectable activity below 75 μM (Table 1).

Discovery of four highly active piperidine analogues in the D-sector of **1** (**15a**−**d**, see Table 1 for biological data) encouraged us to further examine this center in an effort to retain nM potency while improving solubility within the series. Thus, morpholine derivative **23a**, piperazines **23b**−**d**, **24e**, and piperidine rings decorated with hydrophilic groups **24f**, **28a**−**d**, and **29e**−**f** were prepared. Unfortunately, with the exception of **28c** bearing a CH_2OH group alpha to nitrogen (EC_{50} 850 nM), none of the compounds are significantly active. Clearly, the incorporation of a hydrophilic group in this sector is detrimental to MV blockade (Table 1). This may reflect impaired passive diffusion through the plasma membrane because inhibitors of the RdRp complex activity need access to the cytosol of the infected cells.

Scheme 1. Synthesis of 1-Methyl-3-(trifluoromethyl)-4-bromo-*N*-[4-(pyrrolidinylsulfonyl)-phenyl]-1*H*-pyrazole-5-carboxamide (**4**)[a]

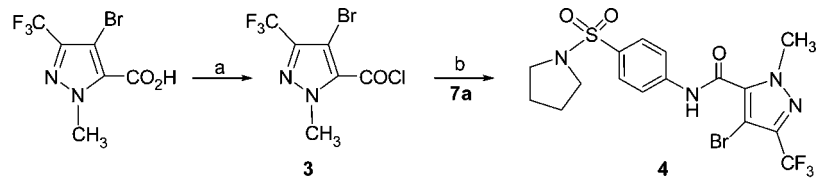

[a] Reagents: (a) $(COCl)_2$, DMF(cat.), CH_2Cl_2, 0°C-rt; (b) 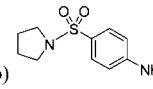 (**7a**), py, CH_2Cl_2, rt.

Scheme 2. Synthesis of 1-Alkyl-3-(trifluoromethyl)-5-carboxamide **9**[a]

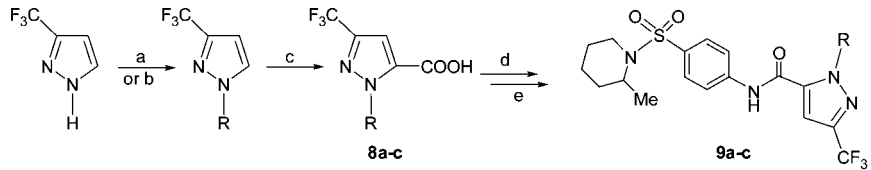

[a] Reagents: (a) NaH, benzyl bromide, DMF; or (b) K_2CO_3, RI, DMF ;(c) *n*-BuLi/*i*-Pr_2NH, then CO_2;

(d) $(COCl)_2$, DMF(cat.), CH_2Cl_2, 0°C-rt; (e) 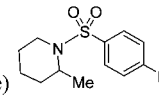 (**7c**), py,CH_2Cl_2, rt.

Scheme 3. Synthesis of 1-[2-Carboxy-phenyl]-3-trifluoromethyl-pyrazole Analogues[a]

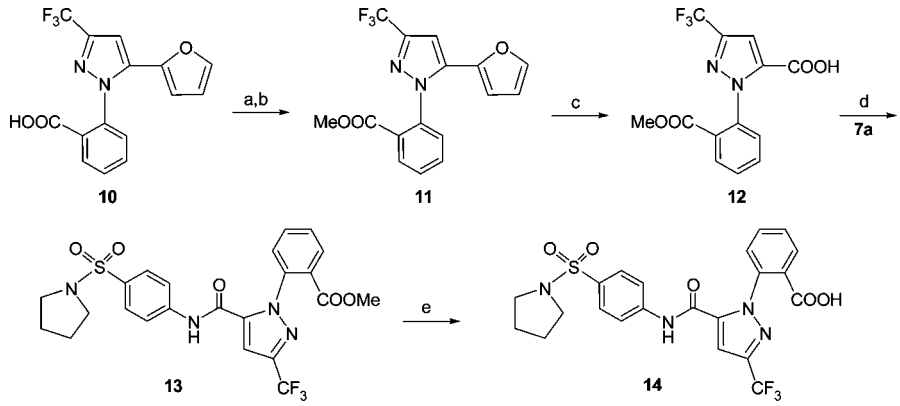

[a] Reagents: (a) oxalyl chloride; (b) MeOH; (c) $KMnO_4$, H_2O, acetone; (d) $(COCl)_2$, DMF (cat.), CH_2Cl_2, 0°C-rt, then py, **7a**, CH_2Cl_2, rt; (e) 50% NaOH, MeOH/H_2O (5:1), room temperature, 5 h, then 1 N HCl.

Molecular Field Topology Analysis (MFTA) QSAR. The SAR discussion in the previous section is based on qualitative observations. In an effort to put this on a more quantitative footing, the MFTA method developed by Palyulin et al.[17,18] was applied to the MV RdRp complex inhibitor series to generate a quantitative structure−activity relationship (QSAR). MFTA performs a topological analysis for a compound series, generates a molecular supergraph with descriptor values for each compound mapped at each atom vertex, and finishes with PLS-based correlation statistics to generate predictive QSAR models. In the present case, the $\log(1/EC_{50})$ values for CPE inhibition without standard deviations were used as the numerical biological end points. To incorporate the virus titer data into the correlation, the titer values of compounds with CPE inhibitory activities less than 2.3 μM were scaled to an equivalent CPE EC_{50} by a conversion factor of 10 μM EC_{50} per 1 μM virus titer. The latter was based on the EC_{50}s and virus titers for **15o** and **28d**. Where compounds exhibit activities greater than 75 μM, a value of 150 μM was assigned. Compounds with a cytoxicity greater than 300 μM or a theraputic index greater than 4 were selected for MFTA. To simplify the analysis within a congeneric series, only compounds with a scaffold similar to the pyrazole ring A, amide linker B, and sulfonamide linker C were included. Thus, the training set consisted of 26 compounds: **1**, **2j**, **2o**, **9a**, **13**, **14**, **15a**, **15c**−**15i**, **15k**, **15m**, **15o**, **15p**, **15r**, **23a**, **23d**, **28c**, and **28d**. Three compounds from a previous publication[15] were also included because they are instructive members of this congeneric series (cf. **S5**, **S7**, and **S8**, Figure S1, Supporting Information). On the other hand, **9b, 23c**, **24f**, **29e**, and **29f** were inactive and consistent outliers. Thus, these compounds were excluded from the training set. For the test set, seven compounds were used **2n**, **2k, 15b, 15n**, **24e, 28a**, and **S6** (Figure S1, Supporting Information).[15]

A variety of single local descriptors and sets of local descriptors were applied to the training set, generating a series of different models with varying predictive Q^2 values based on MFTA's leave-25% cross-validation. The best results were obtained with descriptors for Gasteiger−Marsili atomic charge

Scheme 4. Synthesis of Derivatives **23** and **24**[a]

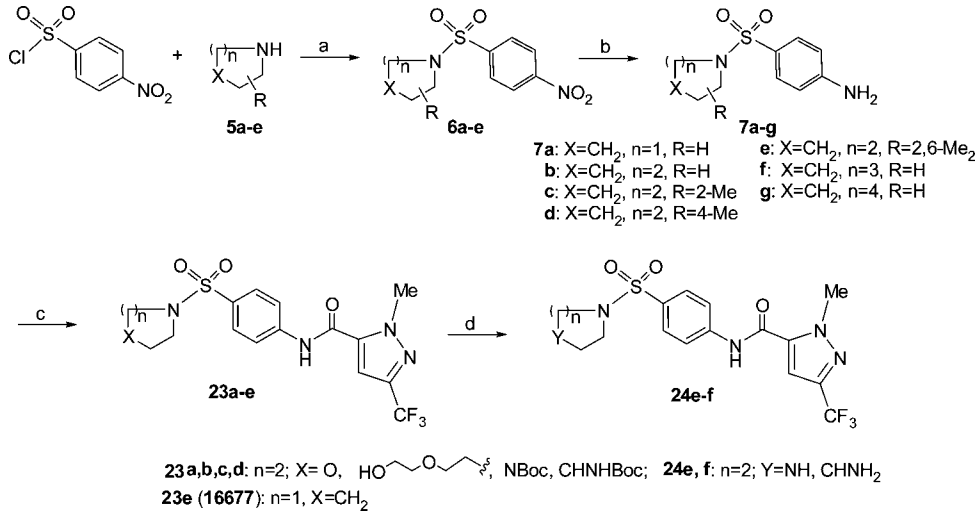

[a] Reagents: (a) Py/CH_2Cl_2; (b) Pd/C (10%), H_2 (50 psi), 1 h; (c)Py, CH_2Cl_2, 1-methyl-3-trifluoro-pyrazole-5-acetyl chloride, 2 h; (d) TFA/CH_2Cl_2 (3:1), 4 h.

Scheme 5. Synthesis of Substituted Piperidine Derivatives **28** and **29**[a]

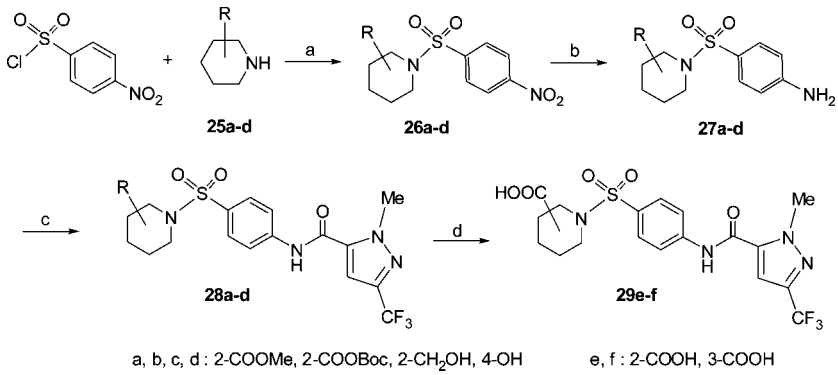

[a] Reagents: (a) Py/CH_2Cl_2; (b) Pd/C (10%), H_2 (50 psi), 1 h; (c)Py, CH_2Cl_2, 2 h; (d) 50% NaOH, MeOH/H_2O (5:1), room temperature, 5 h, then 1 N HCl.

(Q), the effective environment van der Waal radius (R_e), and group lipophilicity based on the sum of the Ghose−Crippen atomic contributions for an atom and attached hydrogens (L_g). This QSAR model generated a correlation (Figure 6) with the following statistics: $N = 26$, number of PLS factors $N_F = 2$, $R = 0.88$, $R^2 = 0.77$, RMSE = 0.49, and $Q^2 = 0.66$. Adding additional descriptors did not substantially improve the correlation. To verify that MFTA has not simply fortuitously found a nonpredictive model, a Y-randomization test[38] was performed on the training set data in ten separate trials. In each trial, the activity data was randomly reordered, and a QSAR model generated. Each random data set delivered the same mean, variance, and molecular supergraph, but no real correlation of activity to structure. The resulting QSAR models generally had a good correlation ($R_{avg} = 0.83$, $R_{max} = 0.92$) but poor predictive ability ($Q^2_{avg} = 0.21$, $Q^2_{max} = 0.42$). This lends confidence that the experimental model with $Q^2 = 0.66$ is not an artifact of the method.

Predictions for the seven compound test set with the present model were made by first using MFTA to map the test set compounds with assigned descriptor values to the previously generated molecular supergraph, followed by prediction with the PLS model based on the training set (Figure 5). Test set activities are predicted reasonably well with $R = 0.67$ and $R^2 = 0.45$. For three of the compounds, the errors are somewhat substantial (about 30−40% of the training set activity span in log units), but for the other four compounds, the error is less than 20%. The mean absolute error for the complete test set is 0.74 log units, and the rms error of prediction is 0.86 log units.

MFTA was used to visualize the descriptors' contributions to the correlation by means of a color-coded molecular supergraph (Figure 6). Positions colored brown and red suggest that an increase in descriptor property in that part of the molecule would increase activity, red positions having more effect than brown. Conversely, light blue and blue positions suggest that an increase in descriptor property would decrease activity, blue positions having more effect than light blue. At uncolored positions, either the descriptor property is not correlated to activity or there is insufficient diversity in the training set for MFTA to develop correlation to activity. The reader should note that the attempt to display the range of substituents in 2D in sector D in Figure 6 leaves the impression of disorder around the sulfonyl amine group. This is inaccurate and misleading because the correlation of descriptor property to activity is limited by the property range of the substituents in the training set. The graph accurately reflects how subtle changes in the atoms' properties affect activity within the bounds of diversity in the training set.

Interpreting the descriptor impact graphs supports qualitative trends in the structure−activity data. Substituted rings and alkyl chains attached to the sulfonamide have a positive impact on activity if they increase the lipophilicity and decrease the charge

Table 1. Antiviral MV EC_{50}'s, Cytotoxicities, and Selectivity Indices for 1-Methyl-*N*-(4-(piperidin-1-ylsulfonyl)phenyl)-3-(trifluoromethyl)-1*H*-pyrazole-5-carboxamide (**15a**) and other sulfonamide analogues

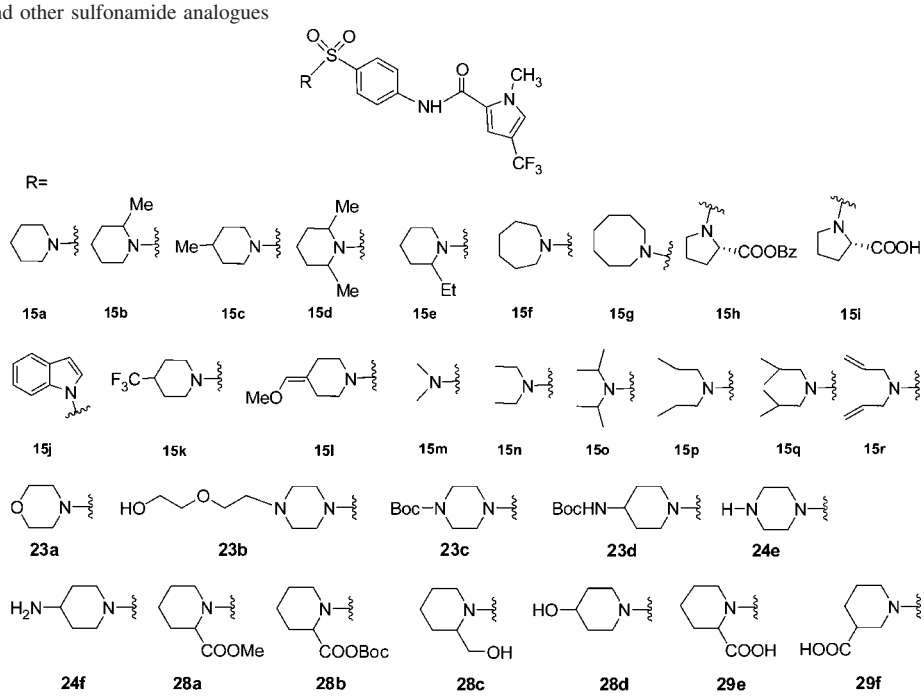

	EC_{50} (μM) (MV-Alaska)		CC_{50} (μM) (Vero cells)		SI (CC_{50}/EC_{50})	
entry ID no.	CPE inhibition[a]	virus titer reduction[c]	MTT cytotoxicity[d]	Trypan blue exclusion assay[e]	CPE + MMT	titer + trypan
4	>75	ND	95 ± 20	ND	<1.3	ND
9a	<2.3	0.055 ± 0.013	30 ± 2.4	ND	ND	ND
9b	>75	ND	>300	ND	ND	ND
9c	>19[c]	>19[b]	ND	19 ± 1	ND	ND
13	>75	>75	ND	>300	ND	ND
14	>75	>75	ND	>300	ND	ND
15a[f]	<2.3	0.014 ± 0.02	>300	199 ± 27	>130	14214
15b	<2.3	0.029 ± 0.031	>300	54 ± 3	>130	1862
15c	<2.3	0.035 ± 0.035	>300	53 ± 4	>130	1514
15d	<2.3	0.014 ± 0.013	>300	328 ± 28	>130	23429
15e	<2.3	0.087 ± 0.116	>300	14 ± 2	>130	160.9
15f	<2.3	0.005 ± 0.0003	>300	425 ± 65	>130	85,000
15g	<2.3	0.045 ± 0.034	16 ± 0.8	ND	>7	ND
15h[f]	14 ± 2	ND	100	ND	7.1	ND
15i[f]	23 ± 10	ND	>300	ND	>13	ND
15j[f]	>13[b]	ND	13 ± 0.7	ND	ND	ND
15k	2.3 ± 0.7	0.02 ± 0.02	159 ± 12	ND	69.1	ND
15l	>75	ND	92 ± 9.3	ND	<1.2	ND
15m	6.3 ± 0.6	ND	>300	ND	>47.6	ND
15n	<2.3	0.019 ± 0.019	>300	280 ± 90	>130	14737
15o	3.5 ± 0.4	0.53 ± 0.02	>300	ND	>85.7	ND
15p	<2.3	0.19 ± 0.32	>300	ND	>130	ND
15q	>13.8[b]	ND	13.8 ± 0.7	ND	ND	ND
15r	3.3 ± 1.4	ND	34 ± 0.9	ND	10.3	ND
16	>15[b]	ND	15 ± 0.6	ND	ND	ND
17	>75	ND	>300	ND	ND	ND
18	>75	ND	286 ± 17	ND	<3.8	ND
19	>75	ND	84 ± 23	ND	<1.1	ND
20	>75	ND	>300	ND	ND	ND
23a[f]	43 ± 24	ND	>300	ND	>7	ND
23b	>75	ND	>300	ND	ND	ND
23c	>75	ND	>300	ND	ND	ND
23d	14.1 ± 6.6	ND	>300	ND	>21.3	ND
24e	28 ± 9	ND	126 ± 7	ND	4.5	ND
24f[f]	>75	ND	>300	ND	ND	ND
28a	10 ± 5.6	ND	136 ± 3	ND	13.6	ND
28b	>38[b]	ND	38 ± 1	ND	ND	ND
28c	<2.3	0.85 ± 0.05	159 ± 40	ND	>69	ND
28d	6.8 ± 0.9	0.57 ± 0.04	274 ± 19	ND	40.2	ND
29e	>75	ND	>300	ND	ND	ND
29f	>75	ND	>300	ND	ND	ND

[a] EC_{50}not determined (ND) when $CC_{50} \leq 15$ μM. Values represent averages of four experiments ± SD; highest concentration assessed 75 μM, lowest concentration assessed 2.3 μM. [b] No virus inhibition detected at CC_{50} concentration. [c] Determined only when CPE inhibition-based EC_{50} concentration <2.3 μM. Values represent averages of two to four experiments ± SEM; highest concentration assessed 1 μM. (ND: not determined) [d] Values represent averages of at least three experiments ± SD; highest concentration assessed 300 μM. [e] Determined only when virus titer reduction was assessed and MTT-assay based cytotoxicity >300 μM. (ND: not determined) [f] Published results.[15]

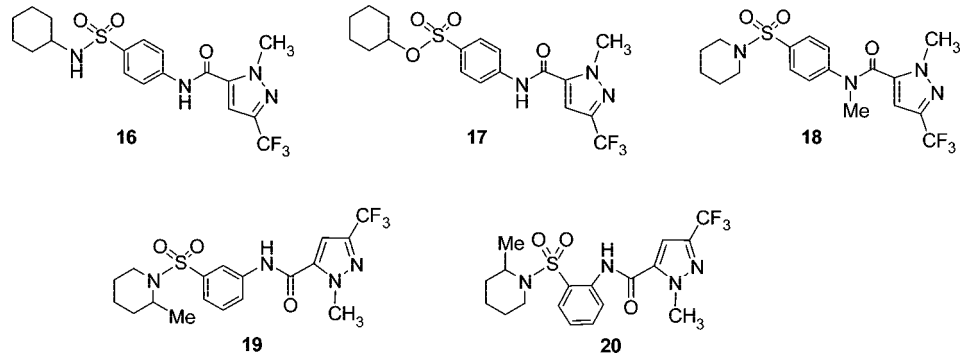

Figure 3. Variation scaffolds of piperidine analogues.

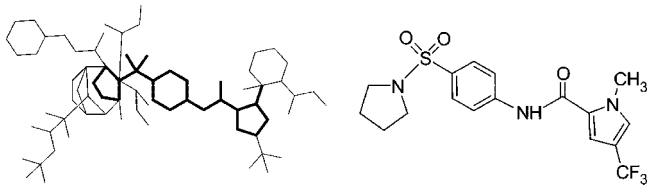

Figure 4. MFTA molecular supergraph (left) formed by the 26 compounds of the training set. The superposition of compound **1** (right) is highlighted to exemplify the alignment.

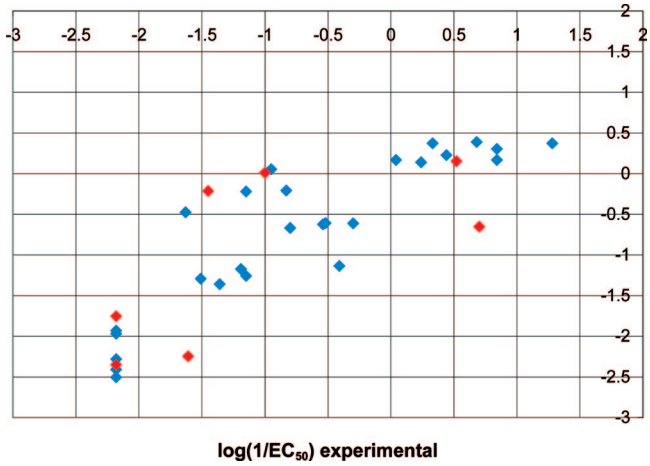

Figure 5. MFTA correlation for the 26 compounds of the training set (blue) and the seven compounds of the test set (red) based on charge (Q), effective vdW radius (R_e), and lipophilicity (L_g) descriptors.

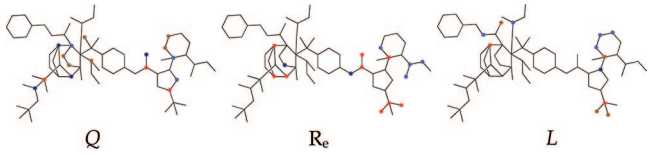

Figure 6. Descriptor impact on activity shown on the molecular supergraph. The QSAR model predicts that increasing the descriptor property at the red and blue positions results in an increase and decrease in activity, respectively.

on this part of the molecule. However, the QSAR model is able to parse some additional complexity in the structure−activity data by noting that increasing charge in the 3- and 4-positions of the pyrrolidine ring, as well as the *para*-position of the six-membered ring, has a favorable effect on activity. In general, substituents connected to the pyrazole ring have a favorable impact on activity if they contribute an increase in size and lipophilicity. Increasing charge at the pyrazole ring can either positively or negatively effect activity, depending on the substituent position.

Discussion

Mechanistic and functional characterization of the high-throughput screening hit **1** has demonstrated that the compound represents a first-in-class non-nucleoside inhibitor of MV RdRp complex activity.[13] We have developed an SAR by structural manipulation of **1** within the four sectors highlighted in Figure 2a. As an extension of previously published work[15] mainly focusing on the phenyl sulfonamide unit, the amide linker, and the pyrazole ring in sector A, the current modification within sector A–C either essentially abolish anti-MV activity or result in high cytotoxicity. However, a highly potent analogue has been identified by replacing the pyrrolidine ring in compound **1** with a piperidine. Subsequent SAR development of the current series was centered on modification of the heterocyclic rings in sectors A and C. Disappointedly, all attempts to replace the *N*-methyl group on the pyrazole ring (**9a**−**c**, **13**, and **14**) or to add other functionality on the same ring leads to complete loss of activity or high toxicity (**9a**). Furthermore, replacement of the pyrazole ring CF_3 group with Me or *t*-Bu also causes significant loss of activity, a factor explained below by the beneficial electrostatic properties of the CF_3 group.

Intriguingly, maintaining the structure of the hit molecule **1** in sectors A−C, while modifying the pyrrolidine ring in D, delivers highly active and noncytotoxic compounds. (Table 1, **15a**−**g**, **15k**) The seven-membered ring analogue **15f** was the most potent series member with an EC_{50} around 5 nM and no detectable cytotoxicity at concentrations below 300 μM as determined by two independent assays (reflected by an approximate selectivity index (CC_{50}/EC_{50}) of 85000). Further increases in the ring size, however, resulted in a reduction of antiviral activity by about 10-fold (Table 1, **15g**). The open-chain diethyl amine analogue **15n** also exhibited excellent antiviral activity. However, other amine substitutions (**15o** and **15q**) caused a complete loss of activity.

Further optimization of the lead compound sought to increase solubility and improve cellular bioavailability. Such structural changes may, of course, reduce membrane permeability and consequently compromise antiviral activity. In attempts to resolve the conflicting structural requirements, compounds with a piperazine ring (**24e**) and polar groups on the piperidine (e.g., **24d**,**f** and **28a**−**f**, Figure 2a, sector D) were prepared. Indeed, assessment of biological activity returned a correlation between increasing hydrophilicity and decreasing inhibitory potency. Within this series, all compounds were completely inactive with the exception of piperidines **28c** and **28d**, which harbor 2-CH_2OH and 4-OH groups, respectively; both returning only moderate activity.

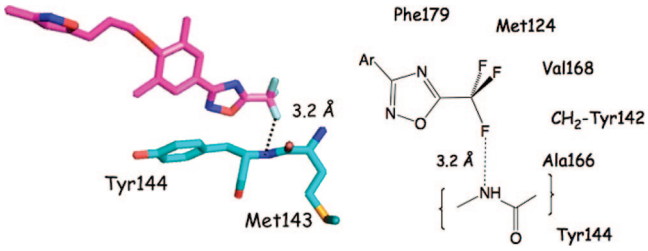

Figure 7. The 1,2,4-oxadiazole terminus of the rhinovirus blocker pleconaril sited in a hydrophobic pocket as determined by X-ray crystallography (1NCR). One of the CF_3 fluorine atoms engages in a slightly elongated hydrogen bond with the backbone NH of Tyr144.

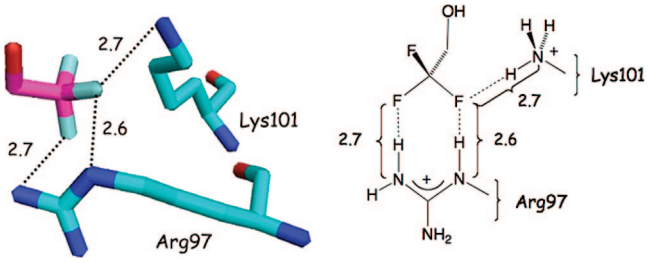

Figure 8. H-Ras 166 in 50% 2,2,2-triflouroethanol (1P2S) sequesters the CF_3 group of a solvent molecule between Arg97 and Lys101 side chains by bidentate and monodentate hydrogen bonds, respectively. Distances are between F—N atoms. Units for numerical values are Å.

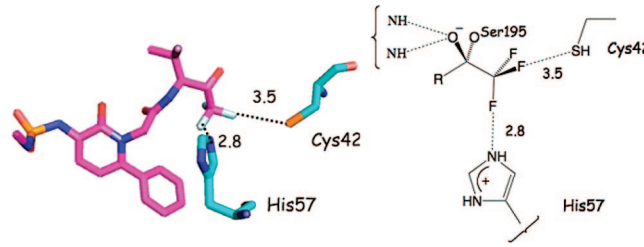

Figure 9. A trifluoromethyl ketone inhibitor of human leukocyte elastase (1EAS) illustrating an F—HS hydrogen bond and a charge dipole interaction between a ligand C—F bond and His57. Units for numerical values are Å.

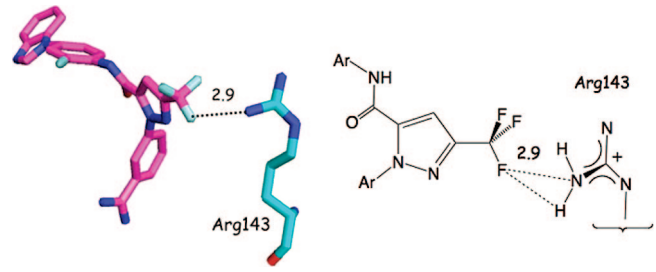

Figure 10. Porcine factor IXa complexed to 1-{3-[amino(imino)-methyl]phenyl}-*N*-[4-(1*H*-benzimidazol-1-yl)-2-fluorophenyl]-3-(trifluoromethyl)-1*H*-pyrazole-5-carboxamide) (1 × 7A). The CF3 of the pyrazole ligand interacts tightly with the cationic terminus of the Arg143 side chain. Units for numerical values are Å.

Interactions between Ligand CF_3 Groups Associated Proteins. Compound **1**, the most potent high-throughput screening (HTS) inhibitor against MV,[13] identified from a 34000 compound pool,[19] carries a trifluoromethyl group on the pyrazole ring. Substitution of the CF_3 with a methyl or a *t*-butyl group completely abrogates the inhibitory activity of the compound.[15] To gain insight into the possible role of the pyrazole CF_3 as an enhancer of MV inhibition and to investigate more generally the structural influence of CF_3 groups in protein-bound ligands, we searched the Protein Data Bank (PDB) for such protein—ligand complexes using Relibase+ and ReliView. A total of 132 CF_3-complemented ligands was returned from the search. Less than a dozen trifluoromethyl groups are located in hydrophobic environments, while 15 are directed into the aqueous layer surrounding the proteins. Carbon—fluorine bonds in 117 complexes were judged to participate in at least one CF—HX (X = O, N, or S, *r*(F—H) 1.8—2.0 Å) interaction in which F—X distances range from 2.7—3.6 Å. It has been argued that fluorine rarely engages in hydrogen bonds in small molecule X-ray crystal structures.[20] However, in protein pockets where ligands are immobilized by a variety of forces, they appear to be more common. F—X distances beyond 3.0 Å can be regarded as dipole—dipole interactions that most likely provide small stabilizing contributions (<1 kcal/mol) for the observed binding poses. An example is presented in Figure 7 showing the heterocyclic terminus of the rhinovirus blocker pleconaril encased in a hydrophobic pocket (PDB code 1NCR[21]). One of the CF_3 fluorine atoms experiences a short contact with the backbone NH of Tyr144.

A subset of 28 cases involve cationic Arg, Lys, and His residues that direct N—H bonds toward fluorine. One interesting CF_3—protein association (1P2S[22]) locates the fluorinated moiety of 2,2,2-trifluoroethanol (CF_3CH_2OH) between Arg and Lys side chains in H-Ras 166 as shown in Figure 8.

The topographical representation shows that Arg97 forms a bidentate contact with two fluorine atoms, while Lys101 associates with one fluorine in the same pair, all of which involve F—H distances of 2.6—2.7 Å. The latter are 0.3—0.4 Å smaller than the sum of the van der Waals radii (N 1.55, F 1.47 Å).[23] These charge—dipole interactions are well-known to operate as controlling forces in the conformational preferences of fluorinated piperidines. In particular, the fluorine in protonated 3-fluoropiperidines universally adopts an axial orientation contrary to intuition based on cyclohexane conformational analysis.[24,25]

Figure 9 depicts a trifluoromethyl ketone inhibitor of human leukocyte elastase (1EAS[26]). The compound enjoys a weak interaction with the SH of Cys42 and a stronger association with His57. Intriguingly, four protein—ligands incorporate CF_3-subsituted pyrazole rings, very similar to that found in compound **1**. Three of these (1 × 7A,[27] 1CX2,[28] and 6COX[29]) juxtapose the CF_3 fluorines and a single Arg residue located among hydrophobic residues. This observation has been exploited to explain the activity of a series of anti-inflammatory COX inhibitors.[30] Porcine factor IXa complexed to 1-{3-[amino(imino)methyl]phenyl}-*N*-[4-(1*H*-benzimidazol-1-yl)-2-fluorophenyl]-3-(trifluoromethyl)-1*H*-pyrazole-5-carboxamide) (1 × 7A) is illustrative (Figure 10). The fourth CF_3-substituted pyrazole ligand, a nanomolar inhibitor of carbonic anhydrase (1OQ5[30]) positions the trifluoromethyl group in a hydrophobic cavity on the surface of the protein partially exposed to the aqueous layer surrounding the protein.

If the binding site for pyrazole in the MV RNA-dependent RNA polymerase were hydrophobic or solvent exposed, then substitution of CF_3 in compound **1** with CH_3 (Figure 2b, **2n**) is unlikely to cause complete loss of activity as observed. Consequently, we conclude that the pyrazole-CF_3 in the highly active MV blockers examined in this work (Table 1, **15a—g**, **15k**, **15n**) is likely docked in a pocket that houses either a cationic Arg, His, or Lys. This prediction is being actively

pursued to identify MV blockers that maintain potency but carry improved solubility and bioavailability properties.

Conclusions

High throughput screening followed by chemical synthesis has provided the first highly potent small molecule blockers of the measles virus accompanied by low cell toxicity. Synthetic modification of the **1** lead reveals that both potency gains and structural diversity resides primarily in sector D (Figure 2a). This behavior is captured by a three-descriptor QSAR model developed using molecular field topology analysis (MFTA) and implies the sector D sulfonyl amines reside in a rather tight hydrophobic cavity. Behavior at the other end of the molecule (sector A) suggests that the pyrazole-CF_3 most likely sits in a pocket housing cationic Arg, His, or Lys. These speculations are being actively pursued in an effort to identify MV blockers that maintain potency but carry improved solubility and bioavailability properties suitable for evaluating various MV strains and closely related viruses in animal models.

Experimental Section

General Chemistry. Routine proton and carbon NMR spectra measured during synthesis were obtained on a Varian Inova-400 (400 MHz). Solvents for NMR were deuteriochloroform ($CDCl_3$) (residual shifts: δ 7.26 for ^{1}H and δ 77.7 for ^{13}C) and deuteriomethyl sulfoxide (DMSO-d_6; residual shift: δ 2.5 for ^{1}H). The residual shifts were taken as internal references and reported in parts per million (ppm). TLC and preparative thin-layer chromatographies (PTLC) were performed on precoated, glass-backed plates (silica gel 60 F_{254}; 0.25 mm thickness) from EM Science and were visualized by UV lamp. Column chromatography was performed with silica gel (230−400 mesh ASTM) using the "flash" method. Elemental analyses were performed by Atlantic Microlab Inc. Norcross, Georgia. All solvents and other reagents were purchased from Aldrich Chemical Co., Milwaukee. The reagents were used as received. All reactions were performed under anhydrous nitrogen atmosphere in oven-dried glassware.

General Procedures for Synthesis of 4-Amino-sulfonamide 7. Pyridine (11.0 mmol, 1.1eq) was added to a solution of 4-nitrobenzenesulfonyl chloride (10.0 mmol, 2.22 g) and amine (11.0 mmol, 1.1eq) in CH_2Cl_2 (20 mL) at 0 °C. The reaction mixture was allowed to warm up to room temperature and stirred for 10 h. The reaction was quenched by addition of 1N HCl (15 mL) and extracted with CH_2Cl_2 (3 × 15 mL). The organic solution was dried (Na_2SO_4) and evaporated to obtain 4-nitro-sulfonamide. The latter was subjected to reduction without further purification.

4-Nitro-sulfonamide (1.0 mmol) in EtOAc was stirred with $SnCl_2.2H_2O$ (5.0 mmol) at room temperature for at least 8 h until starting material disappeared by TLC. The reaction mixture was poured into saturated aqueous $NaHCO_3$ (10 mL) and extracted with EtOAc (3 × 20 mL). The EtOAc extracts were washed with saturated aqueous $NaHCO_3$ (10 mL) a second time and dried (Na_2SO_4). Products were purified by chromatography over silica gel.

Compounds **2a**−**o** were synthesized by the same procedure as compound **1**.

Compound 2a(ns-8). ^{1}H NMR (400 MHz, $CDCl_3$) δ: 1.79 (4H, t, J = 6.8 Hz), 3.26(4H,t, J = 6.8 Hz), 7.60−7.69 (4H, m), 7.76−7.86 (5H, m). Anal. Calcd for $C_{18}H_{17}F_3N_2O_3S$: C, 54.27; H, 4.30; N, 7.03. Found: C, 54.26; H, 4.64; N, 7.74.

Compound 2b (ns-9). ^{1}H NMR (400 MHz, $CDCl_3$) δ: 1.78 (4H, t, J = 6.8 Hz), 3.26(4H,t, J = 6.8 Hz), 7.79−7.87 (6H, m), 8.0−8.02 (3H, m), 7.84−7.87 (3H, m). Anal. Calcd for $C_{18}H_{17}F_3N_2O_3S$: C, 54.27; H, 4.30; N, 7.03. Found: C, 54.20; H, 4.32; N, 7.04.

Compound 2c (ns-10). ^{1}H NMR (400 MHz, $CDCl_3$) δ: 1.76−1.80 (4H, m), 3.26 (4H,t, J = 6.8 Hz), 7.69 (1H, t, J = 8.0 Hz)), 7.82−7.88 (5H, m), 8.0 (1H, s), 8.08 (1H, d, J = 7.6 Hz), 8.14 (s, 1H). Anal. Calcd for $C_{18}H_{17}F_3N_2O_3S$: C, 54.27; H, 4.30; N, 7.03. Found: C, 54.01; H, 4.37; N, 7.10.

Compound 2d (as-36b). ^{1}H NMR (600 MHz, $CDCl_3$) δ: 1.77 (4H, t, J = 7.2 Hz), 3.25 (4H,t, J = 6.6 Hz), 4.65 (2H, s), 7.55 (2H, d, J = 7.8 Hz), 7.82 (2H, d, J = 8.4 Hz), 7.85 (2H, d, J = 7.8 Hz), 7.89 (2H, d, J = 7.8 Hz), 7.96 (s, 1H). Anal. Calcd for $C_{18}H_{19}ClN_2O_3S$: C, 57.06; H, 5.05; N, 7.39. Found: C, 56.21; H, 5.18; N, 7.57.

Compound 2e (as-60a). ^{1}H NMR (400 MHz, $CDCl_3$) δ: 1.61 (4H, m), 3.09(4H, m), 7.05−7.11 (4H, m), 7.64−7.76 (5H, m). Anal. Calcd for $C_{17}H_{17}FN_2O_3S$: C, 58.61; H, 4.92; N, 8.04. Found: C, 58.14; H, 5.12; N, 8.08.

Compound 2f (as-36a). ^{1}H NMR (600 MHz, $CDCl_3$) δ: 1.77 (4H, t, J = 6.6 Hz), 3.25 (4H, t, J = 6.6 Hz), 7.66 (2H, d, J = 8.4 Hz), 7.76 (2H, d, J = 7.8 Hz), 7.80−7.84 (4H, m), 8.0 (1H, s). Anal. Calcd for $C_{17}H_{17}BrN_2O_3S$: C, 49.89; H, 4.19; N, 6.84. Found: C, 49.75; H, 4.23; N, 6.84.

Compound 2g (as-40). ^{1}H NMR (400 MHz, $CDCl_3$) δ: 1.79 (4H, m), 3.23(4H, m), 7.37 (1H, dd, J = 20 Hz, J = 11.2 Hz), 7.83−7.89 (4H, m), 8.50 (1H, dd, J = 2.4 Hz, 6.0 Hz), 8.57 (1H, d, J = 11.2 Hz). Anal. Calcd for $C_{18}H_{16}F_4N_2O_3S$: C, 51.92; H, 3.87; N, 6.73. Found: C, 51.69; H, 3.98; N, 6.57.

Compound 2h (as-60b). ^{1}H NMR (400 MHz, $CDCl_3$) δ: 1.78 (4H, t, J = 6.4 Hz), 3.25 (4H, t, J = 6.8 Hz), 6.92 (1H, dd, J = 3.2 Hz, 8.8 Hz), 7.23 (1H, d, J = 3.2 Hz), 7.53 (1H, d, J = 9.2 Hz), 7.80−7.87 (4H, m), 7.96 (s, 1H). Anal. Calcd for $C_{18}H_{19}BrN_2O_4S$: C, 49.21; H, 4.36; N, 6.38. Found: C, 49.18; H, 4.29; N, 6.42.

Compound 2i (as-61d). ^{1}H NMR (400 MHz, DMSO-d_6) δ: 1.78 (4H, t, J = 6.4 Hz), 3.12 (4H, t, J = 6.4 Hz), 6.55 (1H, dd, J = 2.0 Hz, 8.4 Hz), 6.65 (1H, d, J = 8.4 Hz), 7.75 (2H, d, J = 8.8 Hz), 7.92 (4H, d, J = 8.8 Hz), 10.53 (s, 1H). Anal. Calcd for $C_{17}H_{18}ClN_3O_3S$: C, 53.75; H, 4.78; N, 11.06. Found: C, 53.38; H, 4.79; N, 10.44.

Compound 4 (as-101). ^{1}H NMR (400 MHz, $CDCl_3$) δ: 1.74−1.78 (4H, m), 3.21−3.24 (4H, m), 4.25 (3H, s), 7.79−7.84 (4H, m), 8.66 (1H, s). ^{13}C NMR (100 MHz, $CDCl_3$, ppm): 25.41, 42.04, 48.15, 92.22, 120.32, 129.07, 133.34, 135, 20, 140.62, 155.94. Anal. Calcd for $C_{16}H_{16}BrF_3N_4O_3S$: C, 39.93; H, 3.35; N, 11.64. Found: C, 40.20; H, 3.36; N, 11.21.

Compound 9a (jm1-98). ^{1}H NMR (400 MHz, $CDCl_3$) δ: 1.07 (3H, d, J = 7.0 Hz), 1.49−1.60 (9H, m), 2.98 (1H, td, J = 13.3, 2.3 Hz), 3.69 (1H, bd, J = 13.3 Hz), 4.23 (1H, m), 4.65 (2H, q, J = 7.8 Hz), 6.94 (1H, s), 7.70 (2H, d, J = 8.8 Hz), 7.81 (2H, d, J = 8.8 Hz), 7.82 (1H, s). Anal. Calcd for $C_{16}H_{16}BrF_3N_4O_3S$: C, 51.34; H, 5.22; N, 12.61. Found: C, 51.88; H, 5.54; N, 12.22.

Compound 9b (jm1-89b). ^{1}H NMR (400 MHz, $CDCl_3$) δ: 1.06 (3H, d, J = 7.0 Hz), 1.30−1.45 (2H, m), 1.53 (6H, d, J = 7.0 Hz), 1.55−1.60 (4H, m), 2.97 (1H, td, J = 13.3, 2.3 Hz), 3.66 (1H, bd, J = 13.3 Hz), 4.21 (1H, m), 5.48 (1H, m), 6.98 (1H, s), 7.68 (2H, d, J = 8.6 Hz), 7.74 (2H, d, J = 8.6 Hz), 8.12 (1H, s). Anal. Calcd for $C_{16}H_{16}BrF_3N_4O_3S$: C, 52.39; H, 5.50; N, 12.22. Found: C, 52.44; H, 5.51; N, 11.79.

Compound 9c (as-252). ^{1}H NMR (400 MHz, $CDCl_3$) δ: 1.78 (4H, t, J = 6.4 Hz), 3.24(4H, t, J = 6.8 Hz), 5.84 (2H, s), 7.01 (1H, s), 7.28−7.35 (5H, m), 7.70 (2H, d, J = 8.8 Hz), 7.74 (1H,s), 7.83 (2H, d, J = 8.8 Hz). Anal. Calcd for $C_{24}H_{25}F_3N_4O_3S$: C, 56.91; H, 4.97; N, 11.06. Found: C, 56.95; H, 5.09; N, 11.06.

Compound 13 (as-73b). ^{1}H NMR (400 MHz, $CDCl_3$) δ: 1.71−1.74 (m, 4H), 3.19 (t, 4H, J = 6.8 Hz), 3.76 (s, 3H), 7.10 (s, 1H), 7.48 (dd, 1H, J = 1.6 Hz, 7.8 Hz), 7.57 (d, 2H, J = 8.8 Hz), 7.62 (dd, 1H, J = 1.2 Hz, 7.6 Hz), 7.67 (dd, 1H, J = 1.6 Hz, 7.6 Hz), 7.75 (d, 2H, J = 8.8 Hz), 8.04 (dd, 1H, J = 1.6 Hz, 8.0 Hz), 8.30 (s, 1H). Anal. Calcd for $C_{23}H_{21}F_3N_4O_5S$: C, 52.87; H, 4.05. Found: C, 52.63; H, 4.60.

Compound 14 (as-77). ^{1}H NMR (400 MHz, $CDCl_3$) δ: 1.74 (4H, t, J = 6.8 Hz), 3.2 (4H, t, J = 6.8 Hz), 7.15 (s, 1H), 7.52 (1H, d, J = 8.0 Hz), 7.59 (2H, d, J = 8.8 Hz), 7.64 (1H, d, J = 6.8 Hz), 7.71 (2H, d, J = 8.4 Hz), 7.75 (1H, dd, J = 1.6 Hz, 7.8 Hz), 8.11 (1H, dd, J = 1.2 Hz, 7.8 Hz), 8.33 (1H, s). Anal. Calcd for $C_{22}H_{19}F_3N_4O_5S \cdot H_2O$: C, 50.19; H, 4.02; N, 10.64. Found: C, 50.80; H, 4.20; N, 10.13.

Compound 15a (as-136a). ^{1}H NMR (400 MHz, $CDCl_3$) δ: 1.43−1.44 (m, 2H), 1.63−1.66 (m, 4H), 3.02 (t, 2H, J = 3.6 Hz), 4.28 (s, 3H), 6.98 (s, 1H), 7.75 (d, 1H, J = 6.0 Hz), 7.78 (d, 1H, J = 6.0 Hz), 7.84 (s, 1H). Anal. Calcd for $C_{17}H_{19}F_3N_4O_3S$: C, 49.03; H, 4.60; N, 13.45. Found: C, 49.14; H, 4.64; N, 13.40.

Compound 15b (as-125c). ^{1}H NMR (400 MHz, $CDCl_3$) δ: 1.07 (d, 3H, J = 4.8 Hz), 1.30−1.37 (m, 1H), 1.43 (d, 1H, J = 6.0 Hz), 1.51−1.56 (m, 1H), 2.98 (dt, 1H, J1 = 8.8 Hz, J_2 = 1.6 Hz), 3.64 (d, 1H, 8.0 Hz), 7.16 (s, 1H), 7.78−7.81 (m, 4H), 8.57 (br, 1H). ^{13}C NMR (100 MHz, $CDCl_3$, ppm): 15.61, 18.23, 25.33, 30.47, 40.54, 40.59, 48.91, 105.98, 120.02, 120.62, 121.81, 128.22, 136.38, 136.79, 141.00, 157.38. Anal. Calcd for $C_{18}H_{21}F_3N_4O_3S$: C, 50.23; H, 4.92; N, 13.02. Found: C, 50.34; H, 5.00; N, 12.71.

Compound 15c (as-127). ^{1}H NMR (400 MHz, $CDCl_3$) δ: 0.99 (d, 3H, J = 3.6 Hz), 1.33−1.36 (m, 4H), 1.76 (d, 2H, J = 7.6 Hz), 2.36 (t, 2H, J = 7.8 Hz), 3.79 (d, 2H, J = 8.0 Hz), 4.35 (s, 3H), 7.26 (s, 1H), 7.76 (d, 2H, J = 6.0 Hz), 7.89 (d, 2H, J = 5.6 Hz), 8.73 (br, 1H). ^{13}C NMR (100 MHz, $CDCl_3$, ppm): 21.58, 30.20, 33.35, 40.60, 46.64, 106.03, 120.52, 128.92, 131.32, 141.54, 157.47. Anal. Calcd for $C_{18}H_{21}F_3N_4O_3S$: C, 50.23; H, 4.92; N, 13.02. Found: C, 50.14; H, 4.99; N, 12.86.

Compound 15d (as-125b). ^{1}H NMR (400 MHz, $CDCl_3$) δ: 1.35 (6H, d, J = 7.2 Hz), 1.45−1.55 (m, 6H), 4.17−4.22 (m, 2H), 4.27 (s, 3H), 6.97 (s, 1H), 7.70 (d, 2H, J = 8.8 Hz), 7.80 (s, 1H), 7.83 (d, 2H, J = 8.8 Hz). Anal. Calcd for $C_{19}H_{23}F_3N_4O_3S$: C, 51.34; H, 5.22; N, 12.61. Found: C, 51.41; H, 5.34; N, 12.15.

Compound 15e (yy-0169a). ^{1}H NMR (400 MHz, $CDCl_3$) δ: 0.87 (3H, t, J = 7.2 Hz), 1.41−1.69 (8H, m), 2.96−3.03 (1H, m), 3.73−3.77 (1H, m), 3.91−3.96 (1H, m), 4.27 (3H, s), 7.01 (1H, s), 7.70 (2H, d, J = 8.8 Hz), 7.82 (2H, d, J = 8.8 Hz), 7.95 (1H, s). Anal. Calcd for $C_{19}H_{23}F_3N_4O_3S$: C, 51.34; H, 5.22; N, 12.61. Found: C, 51.36; H, 5.24; N, 12.50.

Compound 15f (as-124a). ^{1}H NMR (400 MHz, $CDCl_3$) δ: 1.56−1.59 (m, 4H), 1.66−1.70 (m, 4H), 3.26 (4H, t, J = 6.0 Hz), 4.26 (s, 3H), 7.10 (s, 1H), 7.69−7.73 (m, 4H), 8.27 (s, 1H). ^{13}C NMR (100 MHz, $CDCl_3$, ppm): 27.07, 29.28, 40.68, 48.45, 120.62, 128.32, 135.52, 136.31, 140.73, 157.28. Anal. Calcd for $C_{18}H_{21}F_3N_4O_3S$: C, 50.23; H, 4.92; N, 13.02. Found: C, 49.71; H, 4.92; N, 12.78.

Compound 15g (as-124f). ^{1}H NMR (400 MHz, $CDCl_3$) δ: 1.62−1.71 (m, 10H), 3.12 (4H, t, J = 4.0 Hz), 4.25 (s, 3H), 7.14 (s, 1H), 7.65−7.69 (m, 4H), 8.42 (br, 1H). ^{13}C NMR (100 MHz, $CDCl_3$, ppm): 25.19, 26.71, 27.88, 40.61, 48.95, 105.91, 120.81, 121.80, 128.37, 134.54, 136.34, 140.86, 157.36. Anal. Calcd for $C_{19}H_{23}F_3N_4O_3S$: C, 51.34; H, 5.22; N, 12.61. Found: C, 51.43; H, 5.27; N, 12.29.

Compound 15j (as-103). ^{1}H NMR (400 MHz, $CDCl_3$) δ: 2.91 (t, 2H, J = 8.0 Hz), 3.93 (t, 2H, J = 8.6 Hz), 4.24 (s, 3H), 6.96 (d, 1H, J = 7.2 Hz), 7.0 (dd, 1H, J = 1.2 Hz, 7.6 Hz), 7.09 (d, 1H, J = 7.6 Hz), 7.20 (t, 1H, J = 7.6 Hz), 7.62 (d, 1H, J = 8.4 Hz), 7.66−7.69 (m, 2H), 7.78−7.81 (m, 2H), 7.87 (s, 1H). ^{13}C NMR (100 MHz, $CDCl_3$, ppm): 28.07, 40.61, 50.21, 105.34, 115.17, 120.14, 124.22, 125.45, 128.02, 128.97, 131.96, 141.35. Anal. Calcd for $C_{20}H_{17}F_3N_4O_3S$: C, 53.33; H, 3.80; N, 12.44. Found: C, 52.92; H, 3.57; N, 12.18.

Compound 15k (yy-0187a). 1H NMR (400 MHz, $CDCl_3$) δ: 1.63−1.66 (1H, m), 1.84−1.87 (1H, m), 1.99−2.04 (1H, m), 2.19−2.25 (2H, m), 2.23−2.25 (1H, m), 3.79−3.82 (1H, m), 3.96−3.98 (1H, m), 4.21−4.23 (1H, m), 4.26 (3H, s), 7.05 (1H, s), 7.73 (2H, d, J = 8.8 Hz), 7.81 (2H, d, J = 8.8 Hz), 8.20 (1H, s). Anal. Calcd for $C_{18}H_{18}F_6N_4O_3S$: C, 44.63; H, 3.75; N, 11.57. Found: C, 44.70; H, 3.76; N, 11.32.

Compound 15l (as-625). ^{1}H NMR (400 MHz, $CDCl_3$) δ: 2.43 (2H, t, J = 6.0 Hz), 2.67 (2H, t, J = 6.0 Hz), 3.14 (2H, t, J = 6.0 Hz), 3.21 (2H, t, J = 6.0 Hz), 3.78 (3H, s), 4.27 (3H, s), 7.0(1H, s), 7.77 (4H, br), 7.88 (1H, s). HRMS calcd for $C_{18}H_{20}F_3N_5O_4S$, 457.12831; found, 458.11204 M + 1. Anal. Calcd for $C_{18}H_{20}F_3N_5O_4S$: C, 47.06; H, 4.39; N, 15.24. Found: C, 46.51; H, 4.39; N, 14.57.

Compound 15m (yy-0233a). ^{1}H NMR (400 MHz, $CDCl_3$) δ: 2.72 (6H, s), 4.28 (3H, s), 7.01 (1H, s), 7.76−7.80 (4H, s), 7.95 (1H, s). Anal. Calcd for $C_{14}H_{15}F_3N_4O_3S$: C, 44.68; H, 4.02; N, 14.89. Found: C, 44.86; H, 4.04; N, 14.62.

Compound 15n (as-154). ^{1}H NMR (600 MHz, $CDCl_3$) δ: 1.14 (t, 6H, J = 7.2 Hz), 3.24 (q, 4H, J = 7.2 Hz), 4.27 (s, 3H), 7.0 (s, 1H), 7.70 (d, 1H, J = 8.4 Hz), 7.79 (d, 1H, J = 9.0 Hz), 7.92 (s, 1H). Anal. Calcd for $C_{16}H_{19}F_3N_4O_3S$: C, 47.52; H, 4.74; N, 13.85. Found: C, 47.41; H, 4.72; N, 13.81.

Compound 15o (yy-0213a). ^{1}H NMR (400 MHz, $CDCl_3$) δ: 1.27 (12H, d, J = 7.2 Hz), 3.68−3.71 (2H, m), 4.27 (3H, s), 7.05 (1H, s), 7.64 (2H, d, J = 8.8 Hz), 7.80 (2H, d, J = 8.8 Hz), 8.02 (1H, s). Anal. Calcd for $C_{18}H_{23}F_3N_4O_3S$: C, 49.99; H, 5.36; N, 12.96. Found: C, 50.18; H, 5.38; N, 12.86.

Compound 15p (yy-0237a). ^{1}H NMR (400 MHz, $CDCl_3$) δ: 0.88 (6H, t, J = 7.6 Hz), 1.53−1.59 (4H, m), 3.06−3.10 (4H, m), 4.27 (3H, s), 7.00 (1H, s), 7.71 (2H, d, J = 8.8 Hz), 7.80 (2H, d, J = 8.8 Hz), 7.89 (1H, s). Anal. Calcd for $C_{18}H_{23}F_3N_4O_3S$: C, 49.99; H, 5.36; N, 12.96. Found: C, 50.03; H, 5.40; N, 12.86.

Compound 15q (yy-0215a). ^{1}H NMR (400 MHz, $CDCl_3$) δ: 0.88 (12H, d, J = 6.4 Hz), 1.88−1.91 (2H, m), 2.86 (4H, d, J = 7.6 Hz), 7.02 (1H, s), 7.69 (2H, d, J = 8.8 Hz), 7.76 (2H, d, J = 8.8 Hz), 7.96 (1H, s). Anal. Calcd for $C_{20}H_{27}F_3N_4O_3S$: C, 52.16; H, 5.91; N, 12.17. Found: C, 52.18; H, 6.01; N, 12.04.

Compound 15r (yy-0247a). ^{1}H NMR (400 MHz, $CDCl_3$) δ: 3.82 (4H, d, J = 6.8 Hz), 4.28 (3H, s), 5.14−5.18 (4H, m), 5.57−5.65 (2H, m), 6.99 (1H, s), 7.34 (2H, d, J = 8.8 Hz), 7.83 (2H, d, J = 8.8 Hz), 7.88 (1H, s). Anal. Calcd for $C_{18}H_{19}F_3N_4O_3S$: C, 50.46; H, 4.47; N, 13.08. Found: C, 50.33; H, 4.44; N, 12.83.

Compound 16 (as-140). ^{1}H NMR (400 MHz, $CDCl_3$) δ: 1.13−1.27 (m, 4H), 1.54−1.56 (m, 2H), 1.64−1.66 (m, 2H), 1.76−1.78(m, 2H), 3.15−3.16 (m, 1H), 4.27 (s, 3H), 4.34 (d, 1H, J = 5.2 Hz), 6.99 (s, 1H), 7.73 (d, 2H, J = 5.6 Hz), 7.87−7.90(m, 3H). Anal. Calcd for $C_{18}H_{21}F_3N_4O_3S$: C, 50.23; H, 4.92; N, 13.02. Found: C, 50.27; H, 5.03; N, 12.99.

Compound 17 (as-155). ^{1}H NMR (400 MHz, $CDCl_3$) δ: 1.22−1.31 (3H, m), 1.45−1.55 (3H, m), 1.68−1.78 (4H, m), 4.26 (3H, s), 4.51 (m, 1H), 7.1 (s, 1H), 7.77 (d, 1H, J = 8.0 Hz), 7.83 (d, 1H, J = 8.0 Hz), 8.30 (br, 1H). Anal. Calcd for $C_{18}H_{20}F_3N_3O_4S$: C, 50.11; H, 4.67; N, 9.74. Found: C, 50.11; H, 4.58; N, 9.59.

Compound 18 (as-627-03). ^{1}H NMR (400 MHz, $CDCl_3$) δ: 1.38−1.42 (2H, m), 1.58−1.64 (4H, m), 2.88 (4H, t, J = 5.2 Hz), 3.49 (3H, s), 4.15 (3H, s), 5.59 (1H, s), 7.23−7.26 (2H, m), 7.70−7.72 (2H, d, J = 8.4 Hz). Anal. Calcd for $C_{18}H_{21}F_3N_4O_3S$: C, 50.23; H, 4.92; N, 13.02. Found: C, 50.32; H, 4.90; N, 12.78.

Compound 19 (yy-0131b). ^{1}H NMR (400 MHz, $CDCl_3$) δ: 1.05 (3H, d, J = 7.2 Hz), 1.25−1.56 (6H, m), 2.96−3.04 (1H, m), 3.71−3.74 (1H, m), 4.22−4.27 (4H, m), 7.19 (1H, s), 7.50−7.54 (1H,m), 7.58−7.60 (1H, d, J = 8.0 Hz), 7.93−7.97 (1H, m), 8.18 (1H, d, J = 8.0 Hz), 8.64 (1H, br). Anal. Calcd for $C_{18}H_{21}F_3N_4O_3S$: C, 50.23; H, 4.92; N, 13.02. Found: C, 50.29; H, 4.95; N, 13.05.

Compound 20 (yy-0131c). ^{1}H NMR (400 MHz, $CDCl_3$) δ: 1.11 (3H, d, J = 7.2 Hz), 1.25−1.55 (6H, m), 2.99−3.06 (1H, m), 3.60−3.63 (1H, m), 4.16−4.18 (1H, m), 4.31 (3H, s), 7.06 (1H, s), 7.26 (1H, t, J = 8.4 Hz), 7.60 (1H, t, J = 8.4 Hz), 7.86 (1H, d, J = 8.4 Hz), 8.56 (1H, d, J = 8.4 Hz), 10.43 (1H, br). Anal. Calcd for $C_{18}H_{21}F_3N_4O_3S$: C, 50.23; H, 4.92; N, 13.02. Found: C, 50.00; H, 4.92; N, 12.92.

Compound 23a (as-236). ^{1}H NMR (400 MHz, $CDCl_3$) δ: 3.02 (4H, t, J = 4.8 Hz), 3.76 (4H, t, J = 4.8 Hz), 4.28 (s, 3H), 7.0 (s, 1H), 7.82−7.79 (m, 4H), 7.86 (s, 1H). Anal. Calcd for $C_{16}H_{17}F_3N_4O_4S$: C, 45.93; H, 4.10; N, 13.39. Found: C, 45.92; H, 4.19; N, 13.17.

Compound 23b (as-270). ^{1}H NMR (400 MHz, $CDCl_3$) δ: 2.59−2.63 (6H, m), 3.05 (4H, br), 3.53−3.62 (6H, m), 4.27 (3H, s), 7.14 (1H, s), 7.65 (2H, d, J = 8.8 Hz), 7.75 (2H, d, J = 8.8 Hz), 8.69 (1H, s). ^{13}C NMR (100 MHz, $CDCl_3$, ppm): 40.74, 46.02, 52.40, 54.19, 57.49, 61.93, 67.48, 72.14, 105.88, 120.17, 129.13, 130.72, 136.36, 141.90, 157.30. Anal. Calcd for $C_{20}H_{26}F_3N_5O_5S \cdot H_2O$: C, 45.88; H, 5.39; N, 13.38. Found: C, 46.40; H, 5.08; N, 13.30.

Compound 23c (as-254). ^{1}H NMR (400 MHz, DMSO) δ: 1.33 (9H, s), 2.84−2.85 (4H, m), 3.38 (4H, m), 4.17 (3H, s), 7.56

(1H, s), 7.75 (2H, d, J = 8.8 Hz), 8.01 (2H, d, J = 8.8 Hz), 10.80 (1H, s).

Compound 23d (yy-0168a). ^{1}H NMR (400 MHz, $CDCl_3$) δ: 1.25−1.34 (2H, m), 1.43(9H, s), 1.75−1.80 (2H, m), 2.76−2.86 (2H, m), 3.30−3.33 (1H, m), 3.90−3.97 (2H, s), 4.28 (3H, s), 4.36 (1H, d, J = 8 Hz), 6.97 (1H, s), 7.76 (2H, d, J = 7.2 Hz), 7.89 (1H, s), 7.91 (2H, d, J = 7.2 Hz).

Compound 24e (as-244). ^{1}H NMR (400 MHz, $CDCl_3$) δ: 2.90−2.92 (4H, m), 2.96−2.98 (4H, m), 4.25 (3H, s), 5.28 (1H, s), 7.04 (1H, s), 7.71 (2H, d, J = 9.2 Hz), 7.76 (2H, d, J = 9.2 Hz), 8.17 (1H, s). Anal. Calcd for $C_{16}H_{18}F_3N_5O_3S$: C, 46.04; H, 4.35; N, 16.78. Found: C, 45.58; H, 4.36; N, 16.26.

Compound 24f (yy-0251). ^{1}H NMR (400 MHz, Actone-d_6) δ: 1.33−1.42 (2H, m), 1.65−1.69 (2H, m), 2.49−2.55 (2H, m), 2.93−2.97 (2H, m), 3.14−3.21 (1H, m), 4.25 (3H, s), 7.42 (1H, s), 7.88 (2H, d, J = 8.4 Hz), 7.98 (2H, d, J = 8.4 Hz), 9.96 (1H, s). Anal. Calcd for $C_{17}H_{20}F_3N_5O_3S \cdot 0.5EtOAc$: C, 47.99; H, 5.09; N, 14.73. Found: C, 48.30; H, 5.19; N, 15.21.

Compound 28a (yy-0150a). ^{1}H NMR (400 MHz, $CDCl_3$) δ: 1.48−1.49 (1H, m), 1.58−1.77 (3H, m), 2.05−2.13 (1H, m), 3.16−3.24 (1H, m), 3.58 (3H, s), 3.75−3.77 (1H, m), 4.25 (3H, s), 4.75−4.77 (1H, m), 6.99 (1H, s), 7.22 (2H, d, J = 6.8 Hz), 7.78 (2H, d, J = 6.8 Hz), 7.91 (1H, s). Anal. Calcd for $C_{19}H_{21}F_3N_4O_5S$: C, 48.10; H, 4.46; N, 11.81. Found: C, 48.14; H, 4.50; N, 11.66.

Compound 28b (as-248). ^{1}H NMR (400 MHz, $CDCl_3$) δ: 1.38 (9H, s), 1.48−1.78 (5H, m), 2.12 (1H, d, J = 13.6 Hz), 3.27 (1H, dt, J = 12.8 Hz, 3.2 Hz), 3.74 (1H, d, J = 9.2 Hz), 4.27 (3H, s), 4.65 (1H, d, J = 5.2 Hz), 9.96 (1H, s), 7.71 (2H, d, J = 8.8 Hz), 7.81 (2H, d, J = 8.8 Hz).

Compound 28c (as-267). ^{1}H NMR (400 MHz, $CDCl_3$) δ: 1.23−1.62 (6H, m), 2.20 (1H, m), 3.08 (1H, t, J = 13.2 Hz), 3.53−3.59 (1H, m), 3.77 (1H, d, J = 14.0 Hz), 3.84 (1H, t, J = 10.4 Hz), 4.00−4.06 (1H, m), 4.26 (3H, s), 7.11 (1H, s), 7.74−7.81 (4H, m), 8.48 (1H, s). Anal. Calcd for $C_{18}H_{21}F_3N_4O_4S$: C, 48.43; H, 4.74; N, 12.55. Found: C, 48.33; H, 4.84; N, 12.23.

Compound 28d (yy-0194a). ^{1}H NMR (400 MHz, DMSO-d_6) δ: 1.38−1.41 (2H, m), 1.70−1.72 (2H, m), 2.66−2.70 (2H, m), 3.07−3.15 (2H, m), 3.45−3.52 (2H, m), 4.64 (1H, d, J = 3.6 Hz), 7.52 (1H, s), 7.72 (2H, d, J = 8.8 Hz), 7.96 (2H, d, J = 8.8 Hz), 10.74 (1H, s). Anal. Calcd for $C_{17}H_{19}F_3N_4O_4S$: C, 47.22; H, 4.43; N, 12.96. Found: C, 47.43; H, 4.41; N, 12.72.

Compound 29e (as-251). ^{1}H NMR (400 MHz, $CDCl_3$) δ: 1.23−1.62 (6H, m), 2.20 (1H, m), 3.08 (1H, t, J = 13.2 Hz), 3.53−3.59 (1H, m), 3.77 (1H, d, J = 14.0 Hz), 3.84 (1H, t, J = 10.4 Hz), 4.00−4.06 (1H, m), 4.26 (3H, s), 7.11 (1H, s), 7.74−7.81 (4H, m), 8.48 (1H, s). Anal. Calcd for $C_{18}H_{19}F_3N_4O_5S$: C, 46.95; H, 4.16; N, 12.17. Found: C, 47.10; H, 4.33; N, 11.54.

Compound 29f (yy-0173a). ^{1}H NMR (400 MHz, $CDCl_3$) δ: 1.55−1.70 (2H, m), 1.81−1.96 (2H, m), 2.63−2.74 (2H, m), 2.84−2.89 (1H, m), 3.42−3.45 (1H, m), 3.65−3.67 (1H, m), 4.27 (3H, s), 7.00 (1H, s), 7.78−7.82 (4H, m), 7.94 (1H, broad). Anal. Calcd for $C_{18}H_{19}F_3N_4O_5S$: C, 46.95; H, 4.16; N, 12.17. Found: C, 46.71; H, 4.16; N, 11.42.

Computational Methods. QSAR by Molecular Field Topology Analysis (MFTA). MFTAWin software (version 3.0 beta17) was applied by first performing a topological alignment of the training set structures (compounds **1**, **2j**, **2o**, **9a**, **13**, **14**, **15a**, **15c**−**15i**, **15k**, **15m**, **15o**, **15p**, **15r**, **23a**, **23d**, **28c**, and **28d**, plus **3s**, **5**, **7**, and **8** from a previous publication) to construct a molecular supergraph, providing a common reference framework for the chosen descriptor set. Then MFTA's PLS (partial least-squares) regression function was used to build statistical models, the predictivity of which was assessed by the leave-25%-out cross-validation procedure. A variety of descriptor sets were examined; the best results (high R and Q^2 values, low PLS factor count, small errors) were obtained with descriptors for Gasteiger−Marsili atomic charge (Q), the effective environment van der Waal radius (R_e), and group lipophilicity based on the sum of the Ghose−Crippen atomic contributions for an atom and attached hydrogens (L_g). The veracity of this model was checked by means of an explicit test set (compounds **2n**, **2k**, **15b**, **15n**, **24e**, and **28a**; plus **6** from a previous publication). These compounds were selected based on their range of activities and diversity of structures. MFTA was used to map the test set to the previously generated molecular supergraph and to calculate their descriptor values. Then these values were applied to the previously generated QSAR equation and the test set activities predicted. The validity of the correlation was further checked by randomizing the data and structures. MFTA was also used to generate color-coded molecular supergraphs, reflecting the quantitative effect on activity of each descriptor in each position.

CF_3-Bearing Ligands Bound to Proteins. Identification of CF_3-substituted ligands was achieved by searching the Protein Data Bank (PDB[32]) with Relibase+.[33–35] The resulting 132 hits were individually inspected in ReliView and catalogued for the presence of protein side-chains, water, ions or other small molecules within 4 Å of the fluorine atoms. Selected examples were examined further with DeepView[36] and displayed with PyMOL[37] in the construction of Figures 7–10.

Acknowledgment. This work was supported by a research grant from the American Lung Association, and Public Health Service grants AI056179 and AI071002 from NIH/NIAID (to R.K.P.) and by the National Institutes of Health 1 U54 HG003918 (to J.P.S.). We are grateful to Ernest Murray for synthetic assistance.

Supporting Information Available: Elemental analyses. Compounds **S5**, **S6**, **S7**, and **S8** were reported previously and are pictured here for the reader's convenience.) This material is available free of charge via the Internet at http://pubs.acs.org.

References

(1) Lamb, R. A.; Kolakosky, D. Paramyxoviruses: The viruses and their replication. In *Fundamental Virology*; Fields, B. N., Knipe, D. M., Howley, P. M. , Eds.; Lippencott-Raven: Philadelphia, PA, 1996; pp 577−604.

(2) Hilleman, M. R. Current overview of the pathogenesis and prophylaxis of measles with focus on practical implications. *Vaccine* **2001**, *20*, 651–665.

(3) *Progress in Reducing Measles Mortality— Worldwide, 1999−2003 MMWR Weekly* **2005**, *54*, 200−203.

(4) Gans, H. A.; Arvin, A. M; Galinus, J.; Logan, L; DeHovitz, R.; Maldonado, Y. Deficiency of the humoral immune response to measles vaccine in infants immunized at age 6 months. *J. Am. Med. Assoc.* **1998**, *280*, 527–532.

(5) (a) Polack, F.; P., S. H.; Lee, S; Permar, E; Manyara, H. G.; Nousari, Y.; Jeng, F.; Mustafa, A.; Valsamakis, R. J.; Adams, H. L.; Robinson, D. E; Griffin. Successful DNA immunization against measles: neutralizing antibody against either the hemagglutinin or fusion glycoprotein protects rhesus macaques without evidence of atypical measles. *Nat. Med.* **2000**, *6*, 776–781. (b) Wichmann, O.; Hellenbrand, W.; Sagebiel, D.; Santibanez, S.; Ahlemeyer, G.; Vogt, G.; Siedler, A.; van Treeck, U. Large measles outbreak at a German public school, 2006. *Pediatr. Infect. Dis. J.* **2007**, *26*, 782. (c) Chironna, M.; Prato, R.; Sallustio, A.; Martinelli, D.; Germinario, C.; Lopalco, P.; Quarto, M. Genetic characterization of measles virus strains isolated during an epidemic cluster in Puglia, Italy. *Virol. J.* **2007**, *21*, 90.

(6) Jansen, V. A.; Stollenwerk, N.; Jensen, H. J.; Ramsay, M. E.; Edmunds, W. J.; Rhodes, C. J. Measles outbreaks in a population with declining vaccine uptake. *Science* **2003**, *301*, 804.

(7) Shigeta, S.; Mori, S.; Baba, M.; Ito, M.; Honzumi, K.; Nakamura, K.; Oshitani, H.; Numazaki, Y.; Matsuda, A.; Obara, T.; Shuto, S.; Clercq, E. Antiviral activities of ribavirin, 5-ethynyl-1-β-D-ribofuranosylimidazole-4-carboxamide, and 6′-(*R*)-6′-C-methylneplanocin A against several ortho- and paramyxoviruses. *Antivir. Chem. Chemother.* **1992**, *36*, 435–9.

(8) Gabrielsen, B.; Phelan, M. J.; Barthel-Rosa, L.; See, C.; Huggins, J. W.; Kefauver, D. F.; Monath, T. P.; Ussery, M. A.; Chmurny, G. N.; Schubert, E. M.; Upadhya, K.; Kwong, C.; Carter, D. A.; Secrist, J. A., III; Kirsi, J. J.; Shannon, W. M.; Sidwell, R. W.; Kini, G. D.; Robins, R. K. Synthesis and antiviral evaluation of *N*-carboxamidine-substituted analogs of 1-β-D-ribofuranosyl-1,2,4-triazole-3-carboxamidine hydrochloride. *J. Med. Chem.* **1992**, *35*, 3231–3238.

(9) Barnard, D. L. Inhibitors of measles virus. *Antivir. Chem. Chemother.* **2004**, *15*, 111–119.

(10) Pokrovskii, A. G.; Il'icheva, T. N.; Kotovskaya, S. K.; Romanova, S. A.; Charushin, V. N.; Chupakhin, O. N. Fluorinated Derivatives of Benz[4,5]imidazo[1,2-*b*][1,3] thiazole—Inhibitors of Reproduction of Measles Virus. *Dokl. Biochem. Biophys.* **2004**, *398*, 285–287.

(11) (a) Plemper, R. K.; Erlandson, K. J.; Lakdawala, A. S.; Sun, A.; Prussia, A. J.; Boonsombat, J.; Aki-Sener, E.; Yalcin, I.; Yildiz, I.; Temiz-Arpaci, O.; Tekiner, B.; Liotta, D. C.; Snyder, J. P.; Compans, R. W. *Proc. Natl. Acad. Sci. U.S.A.* **2004**, *101*, 5628–5633. (b) Sun, A.; Prussia, A.; Zhan, W.; Murray, E. E.; Doyle, J.; Cheng, L. T.; Yoon, J. J.; Radchenko, E. V.; Palyulin, V. A.; Compans, R. W.; Liotta, D. C.; Plemper, R. K.; Snyder, J. P. *J. Med. Chem.* **2006**, *49*, 5080–5092.

(12) Plemper, R. K.; Lakdawala, A. S.; Gernert, K. M.; Snyder, J. P.; Compans, R. W. *Biochemistry* **2003**, *42*, 6645–6655.

(13) White, L. K.; Yoon, J.-J.; Lee, J. K.; Sun, A.; Du, Y.; Fu, H.; Snyder, J. P.; Plemper, R. K. Nonnucleoside Inhibitor of Measles Virus RNA-Dependent RNA Polymerase Complex Activity. *Antimicrob. Agents Chemother.* **2007**, *51*, 22932303..

(14) Schlosser, M.; Volle, J.; Leroux, F.; Schenk, K. Switchable Reactivity: The Site-Selective Functionalization of Trifluoromethyl Substituted Pyrazoles. *Eur. J. Org. Chem.* **2002**, 2913–2920.

(15) Sun, A.; Chandrakumar, N.; Yoon, J.-J.; Plemper, R. K.; Snyder, J. P. Nonnucleoside inhibitors of the measles virus RNA-dependent RNA polymerase activity: Synthesis and in vitro evaluation. *Bioorg. Med. Chem. Lett.* **2007**, *17*, 5199–5203.

(16) Pruitt, J. R.; Pinto, D. J. P.; Galemmo, R. A.; Alexander, R. S.; Rossi, K. A.; Wells, B. L.; Drummond, S.; Bostrom, L. L; Burdick, D.; Bruckner, R.; Chen, H.; Smallwood, A.; Wong, P. C.; Wright, M. R.; Bai, S.; Luettgen, J. M.; Knabb, R.; Lam, P. Y.S.; Wexler, R. R. Discovery of 1-(2-Aminomethylphenyl)-3-trifluoromethyl-*N*-[3-fluoro-2′-(aminosulfonyl)[1,1′-biphenyl)]-4-yl]-1*H*-pyrazole-5-carboxamide (DPC602), a Potent, Selective, and Orally Bioavailable Factor Xa Inhibitor. *J. Med. Chem.* **2003**, *46*, 5298–5315.

(17) Palyulin, V. A.; Radchenko, E. V.; Zefirov, N. S. Molecular Field Topology Analysis Method in QSAR Studies of Organic Compounds. *J. Chem. Inf. Model.* **2000**, *40*, 659–667.

(18) Mel'nikov, A. A.; Palyulin, V. A.; Zefirov, N. S. Generation of molecular graphs for QSAR studies. *Dokl. Chem.* **2005**, *402*, 81–85.

(19) ChemDiv, Inc., 6605 Nancy Ridge Drive, San Diego, CA 92121; http://www.chemdiv.com/en/products/screening/.

(20) (a) Dunitz, J. D.; Taylor, R. Organic Fluorine Hardly Ever Accepts Hydrogen Bonds. *Chem.—Eur. J.* **1997**, *3*, 89–98. (b) Dunitz, J. D. Organic Fluorine: Odd Man Out. *ChemBioChem.* **2004**, *5*, 614–621.

(21) Zhang, Y.; Simpson, A. A.; Ledford, R. M.; Bator, C. M.; Chakravarty, S.; Skochko, G. A.; Demenczuk, T. M.; Watanyar, A.; Pevear, D. C.; Rossmann, M. G. Structural and virological studies of the stages of virus replication that are affected by antirhinovirus compounds. *J. Virol.* **2004**, *78*, 11061–11069.

(22) Buhrman, G. K.; de Serrano, V.; Mattos, C. Organic Solvents Order the Dynamic Switch II in Ras Crystals. *Structure* **2003**, *11*, 747–751.

(23) Bondi, A. van der Waals Volumes and Radii. *J. Phys. Chem.* **1964**, *68*, 441–451.

(24) (a) Lankin, D. C.; Chandrakumar, N. S.; Rao, S. N.; Spangler, D. P.; Snyder, J. P. Protonated 3-Fluoropiperidines: An Unusual Fluoro Directing Effect and a Test for Quantitative Theories of Solvation. *J. Am. Chem. Soc.* **1993**, *115*, 3356–3357. (b) Snyder, J. P.; Chandrakumar, N. S.; Sato, H.; Lankin, D. C. The Unexpected Diaxial Orientation of *cis*-3,5-Difluoropiperidine in Water A Potent CF—NH Charge−Dipole Effect. *J. Am. Chem. Soc.* **2000**, *122*, 544–545. (c) Lankin, D. C.; Grunewald, G. L.; Romero, F. A.; Oren, I. Y.; Snyder, J. P. The NH—FC Dipole Orientation Effect for Pendant Exocyclic CH_2F. *Org. Lett.* **2002**, *4*, 3557–3560. (d) Sun, A.; Lankin, D. C.; Hardcastle, K.; Snyder, J. P. 3-Fluoropiperidines and *N*-Methyl-3-fluoropiperidinium Salts: The Persistence of Axial Fluorine. *Chem.—Eur. J.* **2005**, *11*, 1579–1591.

(25) (a) Jensen, H. H.; Lyngbye, L.; Jensen, A.; Bols, M. Stereoelectronic Substituent Effects in Polyhydroxylated Piperidines and Hexahydropyridazines. *Chem.—Eur. J.* **2002**, *8*, 1218–1226. (b) Jensen, H. H.; Bols, M. Stereoelectronic Substitutent Effects. *Acc. Chem. Res.* **2006**, *39*, 259–265.

(26) Bernstein, P. R.; Andisik, D.; Bradley, P. K.; Bryant, C. B.; Ceccrelli, C.; Damewood, J. R., Jr.; Earley, R.; Edwards, P. D.; Feeney, S.; Gomes, B. C.; Kosmider, B. J.; Steelman, G. B.; Thomas, R. M.; Vacek, E. P.; Veale, C. A.; Williams, J. C.; Wolanin, D. J.; Woolson, S. A. Nonpeptidic Inhibitors of Human Leukocyte Elastase. 3. Design, Synthesis, X-ray Crystallographic Analysis, and Structure−Activity Relationships for a Series of Orally Active 3-Amino-6-phenyl-2-pyridinyl Trifluoromethyl Ketones. *J. Med. Chem.* **1994**, *37*, 33133326..

(27) Smallheer, J. M.; Alexander, R. S.; Wang, J.; Wang, S.; Nakajima, S.; Rossi, K. A.; Smallwood, A.; Barbera, F.; Burdick, D.; Luettgen, J. M.; Knabb, R. M.; Wexler, R. R.; Jadhav, P. K. SAR and factor IXa crystal structure of a dual inhibitor of factors IXa and Xa Bioorg. *Med. Chem. Lett.* **2004**, *14*, 5263–5267.

(28) Kurumbail, R. G.; Stevens, A. M.; Gierse, J. K.; McDonald, J. J.; Stegeman, R. A.; Pak, J. Y.; Gildehaus, D.; Miyashiro, J. M.; Penning, T. D.; Seibert, K.; Isakson, P. C.; Stallings, W. C. Structural basis for selective inhibition of cyclooxygenase-2 by anti-inflammatory agents. *Nature* **1996**, *384*, 644–648.

(29) Singh, S. K.; Vobbalareddy, S.; Kalleda, S. R.; Rajjak, S. A.; Casturi, S. R.; Datla, S. R.; Mamidi, R. N. V. S.; Mullangi, R.; Bhamidipati, R.; Ramanujam, R.; Akella, V.; Yeleswarapu, K. R. 2-Hydroxymethyl-4-[5-(4-methoxyphenyl)-3-trifluoromethyl-1*H*-1-pyrazolyl]-1-benzenesulfonamide (DRF-4367): an orally active COX-2 inhibitor identified through pharmacophoric modulation. *Org. Biomol. Chem.* **2004**, *2*, 2442–2450.

(30) Weber, A.; Casini, A.; Heine, A.; Kuhn, D.; Supuran, C. T.; Scozzafava, A.; Klebe, G. Unexpected nanomolar inhibition of carbonic anhydrase by COX-2-selective celecoxib: new pharmacological opportunities due to related binding site recognition. *J. Med. Chem.* **2004**, *47*, 550–557.

(31) Reaction of 4-nitro-benzene sulfonyl chloride with pyrrolidine in the presence of pyridine afforded 4-nitro-prolidinyl sulfonamide. Reduction with tin dichloride dihydrate in ethyl acetate provided 4-amino-prolidinyl sulfonamide **7a** in excellent yield (90%).

(32) Berman, H. M.; Westbrook, J.; Feng, Z.; Gilliland, G.; Bhat, T. N.; Weissig, H.; Shindyalov, I. N.; Bourne, P. E. The Protein Data Bank. *Nucleic Acids Res.* **2000**, *28*, 235–242.

(33) Hendlich, M.; Bergner, A.; Gunther, J.; Klebe, G. Relibase: Design and Development of a Database for Comprehensive Analysis of Protein−Ligand Interactions. *J. Mol. Biol.* **2003**, *326*, 607–620.

(34) Günther, J.; Bergner, A.; Hendlich, M.; Klebe, G. Utilising Structural Knowledge in Drug Design Strategies: Applications Using Relibase. *J. Mol. Biol.* **2003**, *326*, 621–636.

(35) Bergner, A.; Günther, J.; Hendlich, M.; Klebe, G.; Verdonk, M. Use of Relibase for retrieving complex 3D interaction patterns including crystallographic packing effects. *Biopolymers (Nucl. Acid Sci.)* **2002**, *61*, 99–110.

(36) Guex, N.; Diemand, A.; Peitsch, M. C.; Schwede, T. *Swiss-PDB Viewer*; GlaxoSmithKline R&D and the Swiss Institute of Bioninformatics; 2006; http://www.expasy.org/spdbv/.

(37) DeLano, W. L. *The PyMOL Molecular Graphics System*; DeLano Scientific: San Carlos, CA, 2002; http://www.pymol.org.

(38) Wold, S; Eriksson, L., *Chemometric Methods in Molecular Design*; Methods and Principles in Medicinal Chemistry. Vol. 2; van de Waterbeemd, H., Ed.; VCH Publishers, Inc.: New York, 1995; pp 309−317.

JM701239A